Available online at www.sciencedirect.com

SciVerse ScienceDirect

Journal of the European Ceramic Society 32 (2012) 1149–1155

www.elsevier.com/locate/jeurceramsoc

Fe doping and magnetic properties of zincblende SiC ceramics

Kwang Joo Kim [a], Young-Wook Kim [b,*]

[a] Department of Physics, Konkuk University, Seoul 143-701, Republic of Korea
[b] Department of Materials Science and Engineering, The University of Seoul, Seoul 130-743, Republic of Korea

Received 7 October 2011; received in revised form 23 November 2011; accepted 24 November 2011
Available online 15 December 2011

Abstract

Fe-doped SiC bulk ceramics were fabricated by hot-pressing, and their magnetic and electronic properties were investigated. $Si_{1-x}Fe_xC$ ($x \leq 0.04$) samples having a zincblende crystal structure exhibited ferromagnetic hysteresis at room temperature with the saturation magnetization increasing with x. X-ray diffraction measurements revealed the creation of a Fe_3Si phase in the samples with its density increasing with x. The samples were found to be p-type semiconductors with a hole concentration (electrical resistivity) of $\sim 10^{19}$ cm^{-3} ($\sim 10^{0}$ Ω cm) at room temperature. The observed magnetic properties of the samples are mainly ascribed to the presence of ferromagnetic Fe_3Si crystallites. The high carrier concentration of the samples likely implies the existence of acceptors due to individual Fe^{3+} occupation of the Si sites in the lattice. The randomly distributed Fe^{3+} ions represent a minor contribution to the magnetization of the samples through the formation of magnetic polarons with the carriers.
© 2011 Elsevier Ltd. All rights reserved.

Keywords: SiC; Hot pressing; Magnetic properties; Electrical properties

1. Introduction

Silicon carbide (SiC) has a variety of applications ranging from structural materials to electronic devices because of its unique combination of properties such as high thermal stability, high thermal conductivity, variable electrical resistivity, good mechanical strength and corrosion resistance.[1–20] The potential applications of SiC include heat exchangers, fusion reactors, gas-turbine components, pressure sensors and optical mirrors. SiC-based electronic devices can be fabricated to operate under extreme conditions such as high temperature, high power and high frequency, thus, they are suitable for applications in aircrafts and space vehicles.

SiC is known to have many possible crystal structures (polytypes) along with a wide band-gap spectrum covering the visible–ultraviolet range, 2.4, 3.0, 3.3 and 3.4 eV for 3C, 6H, 4H and 2H, respectively.[21] The semiconducting properties of SiC are achieved through the creation of carriers by impurity doping such as N and P for electrons (n-type) and B and Al for holes (p-type).[1,10,19] So far, electrical resistivity as low as 10^{-3} Ω cm has been obtained by N doping in zincblende SiC (3C-SiC).[22] By doping with some magnetic impurities, SiC ceramics may exhibit characteristic magnetic properties as well as a decrease in electrical resistivity.

Relatively little attention has been paid to the doping of 3*d* transition metal (TM) elements in SiC, which can induce ferromagnetism through spin–spin interactions between the TM ions and the carriers. A study based on mean-field theory[23] predicted that some TM-doped semiconductors composed of light elements such as O, N and C occupying the anionic sites can exhibit ferromagnetism at room temperature or higher. Encouraged by the theoretical prediction, semiconductors such as GaN and ZnO with large band-gap energies (~3 eV) have been frequently adopted as hosts for doping TM elements such as Cr, Mn, Fe, Co and Ni.[24]

Only a few studies related to TM doping of SiC materials have been reported to date. Song et al.[25] synthesized Fe-doped 6H-SiC powders that exhibited ferromagnetic behavior above room temperature. Wang et al.[26] observed ferromagnetism persisting near room temperature in a Mn-doped 4H-SiC film. Takano et al.[27,28] observed ferromagnetic ordering in Mn-doped 3C-SiC single crystals. A theoretical investigation of Fe-doped 4H-SiC by Los et al.[29] predicted that paramagnetic and ferromagnetic states might coexist as temperature increases. The covalent distance between Fe and C atoms may be an important factor for determining the preferred magnetic state in SiC polytypes.

* Corresponding author. Tel.: +82 2 2210 2760; fax: +82 2 2215 5863.
E-mail address: ywkim@uos.ac.kr (Y.-W. Kim).

0955-2219/$ – see front matter © 2011 Elsevier Ltd. All rights reserved.
doi:10.1016/j.jeurceramsoc.2011.11.037

Also, ferromagnetic properties recently reported for neutron-irradiated 6H-SiC single crystals were attributed to defects such as divacancies ($V_{Si}V_C$) created by the irradiation.[30]

In this study, Fe-doped SiC ($Si_{1-x}Fe_xC$) ceramics were synthesized and their magnetic and electronic properties were investigated. Structural properties of the prepared bulk samples were investigated by X-ray diffraction (XRD) and scanning electron microscopy (SEM). The magnetic properties of the samples were investigated using a superconducting quantum interference device (SQUID) method. Hall measurements were taken for the samples to determine their semiconducting properties. The experimental results suggest that Fe doping can provide both magnetic moments and carriers to zincblende SiC ceramics.

2. Experimental

The Fe-doped SiC samples were prepared by hot pressing. In order to fabricate the ceramic samples, commercially available β-SiC (grain size ~0.3 μm, Betarundum, Ibiden Co. Ltd., Ogaki, Japan) and Fe powders (grain size 5.0–8.0 μm, International Specialty Products, Inc., Wayne, USA) were used as raw materials. Four different batches were prepared containing β-SiC, Fe, and C powders with Fe compositions (x) of 0.01, 0.02, 0.03 and 0.04 in the formula $Si_{1-x}Fe_xC$. The batches were milled in ethanol for 24 h using SiC grinding balls. The milled slurry was dried, sieved, and hot-pressed at 1850 °C for 1 h under 20 MPa at atmospheric pressure under argon.

The hot-pressed samples were polished and analyzed using SEM and electron probe microanalysis (EPMA, JXA-8500F, JEOL, Tokyo, Japan). The crystal structures of the samples were probed by XRD using Cu Kα radiation. The magnetic hysteresis and temperature-dependent magnetization curves of the samples were measured using SQUID (MPMS5, Quantum Design Inc., San Diego, CA, USA). The electronic properties of the samples were investigated by Hall measurements at room temperature using the van der Pauw method under an external magnetic field of 10 kOe.

Some hot-pressed samples were leached at 80 °C for 5 h using 16% hydrochloric acid for removing Fe_3Si phase.[31] The magnetic hysteresis of the samples was measured again using SQUID at room temperature.

3. Results and discussion

Fig. 1(a) and (b) exhibits magnetic hysteresis (MH) curves of the Fe-doped SiC samples measured using SQUID at 2 and 300 K, respectively, with the external magnetic field (H) being applied parallel to the sample plane. The MH curves imply the persistence of ferromagnetic behavior at room temperature although the magnetization intensity of the sample at 300 K is reduced compared to that at 2 K. The magnetization values at 300 K for $H = 70$ kOe are reduced by 33%, 23%, 25% and 17% compared to those at 2 K for $x = 0.01$, 0.02, 0.03 and 0.04, respectively.

The samples with low Fe content ($x = 0.01$ and 0.02) showed better magnetization saturation at high H compared to those for $x = 0.03$ and 0.04. The effective magnetic moment of each Fe

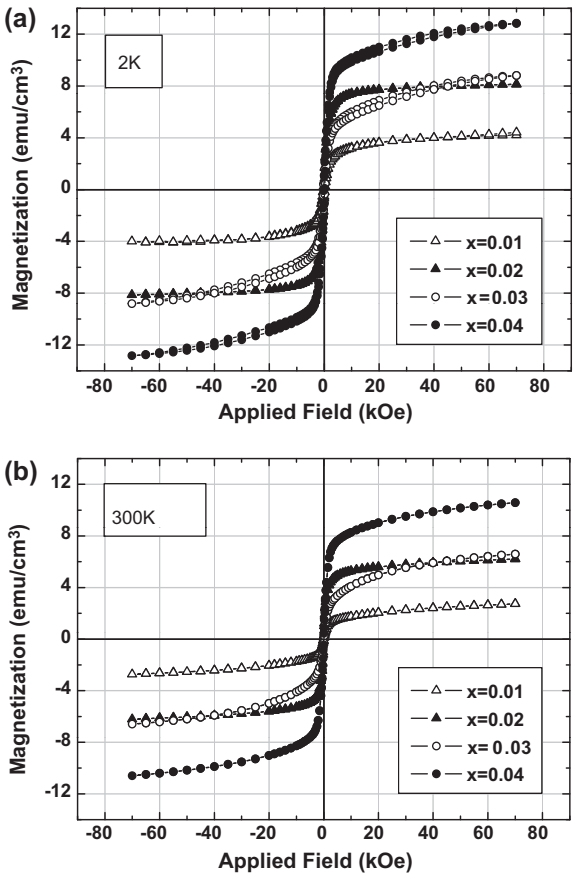

Fig. 1. Magnetic hysteresis curves of Fe-doped zincblende SiC ($Si_{1-x}Fe_xC$) samples measured using SQUID at (a) 2 K and (b) 300 K.

ion for $x = 0.01$ and 0.02 deduced from the observed saturation magnetization at 2 K is 0.9 μ_B if all the Fe ions are assumed to contribute equally. On the other hand, the high-field magnetization for $x = 0.03$ is only slightly larger than that for $x = 0.02$. At low H below 40 kOe, the magnetization for $x = 0.03$ is even smaller than that for $x = 0.02$. Furthermore, the MH curves for $x = 0.03$ and 0.04 show more divergent behavior at high H compared to those for $x = 0.01$ and 0.02. The observed difference in the MH curve shape between the two groups of samples might imply some difference in microstructure between these, which may be related to the magnetic properties.

Fig. 2 exhibits the XRD patterns of the polycrystalline samples, indicating the 3C (zincblende) structure (JCPDS 29-1129). As x increases, a new peak appears at about $2\theta = 45.3°$ as denoted by the arrow. This peak is identified as the (2 2 0) peak of the cubic Fe_3Si phase (JCPDS 45-1207). Fe_3Si is known to be ferromagnetic below the Curie temperature, $T_C = 823$ K,[32] thus, its existence is quite likely to influence the magnetic properties of the samples. The Fe_3Si phase was also detected for Fe-doped 6H SiC powders[25] and crystals.[33] The concurrent appearance of the Fe_3Si-related XRD peak and the change in the MH-curve shape between $x = 0.02$ and 0.03 likely indicates that the change in magnetic behavior is due to a significant increase in the Fe_3Si content between the two Fe compositions. Ferromagnetism observed in Mn-doped 3C-SiC single crystal was also ascribed to the formation of Mn_5Si_2:C clusters.[28]

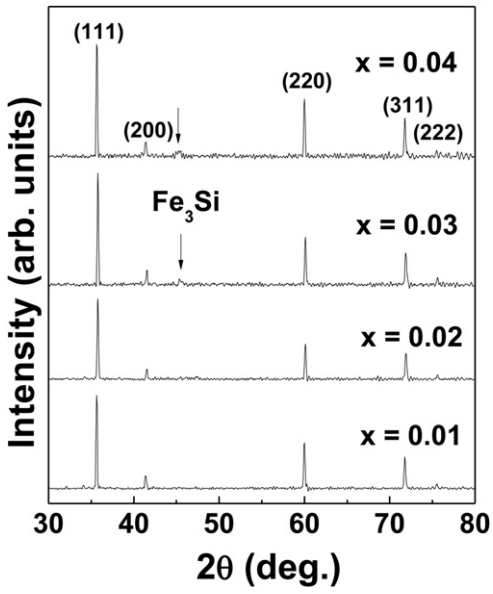

Fig. 2. XRD patterns of $Si_{1-x}Fe_xC$ samples.

Typical fracture surfaces of the samples are shown in Fig. 3. Mostly transgranular fracture is observed in all samples and the grain size increased with increasing x. It seems that the added Fe formed a liquid during sintering and resulted in SiC grain growth. In order to accelerate grain growth of SiC in the presence of liquid Fe, SiC should have some solubility in liquid Fe. Rein and Chipman[34] reported the free energy of SiC from its solubility in Fe, indicating the possibility of a SiC solution in liquid Fe. Fig. 4 shows dot mapping results for Fe obtained by EPMA on the samples with $x = 0.01$ and 0.04. It is evident that the distribution of Fe is not uniform but well concentrated in particular grains in both samples, supporting the Fe_3Si segregation observed on XRD. Thus, the addition of Fe into SiC caused SiC grain growth during sintering and segregated as Fe_3Si by reacting with SiC during cooling. Comparing the distribution of the Fe-segregated spots, the $x = 0.04$ sample (Fig. 4(b)) had a spot density more than four times higher than that of $x = 0.01$ (Fig. 4(a)), supporting the interpretation of the MH result.

Hall measurements revealed that the samples were p-type semiconductors with hole concentrations of 2.2×10^{19}, 1.4×10^{19}, 2.3×10^{19} and $1.9 \times 10^{19}\,cm^{-3}$, respectively, for $x = 0.01$, 0.02, 0.03 and 0.04. The values of the corresponding electrical resistivity are 0.5, 2.0, 1.9 and 1.3 Ω cm, respectively, for $x = 0.01$, 0.02, 0.03 and 0.04. Considering the large band-gap energy of zincblende SiC, the observed carrier concentration ($\sim 10^{19}\,cm^{-3}$) and resistivity ($\sim 10^{0}$ Ω cm) are significant enough to suggest the formation of acceptor levels due to individual Fe substitution into the zincblende lattice sites. According to a total-energy calculation result on 3*d* TM-doped zincblende SiC,[35] the Si sites are strongly preferred substitution sites for the TM elements over the C sites. In Fe-doped SiC, the Fe ions substituting the Si sites are likely to take a valence of +3 with a partially filled *d*-shell of configuration d^5,[25] and these can act as acceptors.

The substituted Fe^{3+} ions having five *d* electrons are also expected to exhibit a magnetic moment. Strong *sp–d* hybridization between the TM and surrounding C atoms is likely to induce a larger ligand-field splitting between *e*- and t_2-states of the *d*

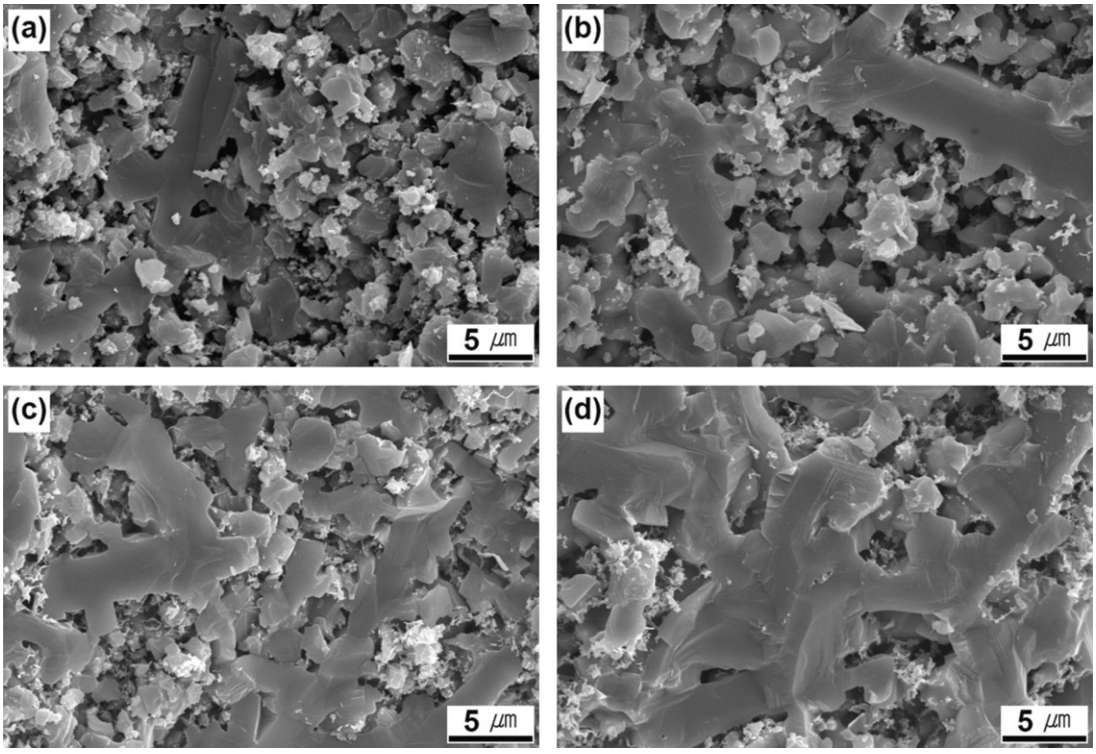

Fig. 3. SEM images of $Si_{1-x}Fe_xC$ samples: (a) $x = 0.01$, (b) $x = 0.02$, (c) $x = 0.03$ and (d) $x = 0.04$.

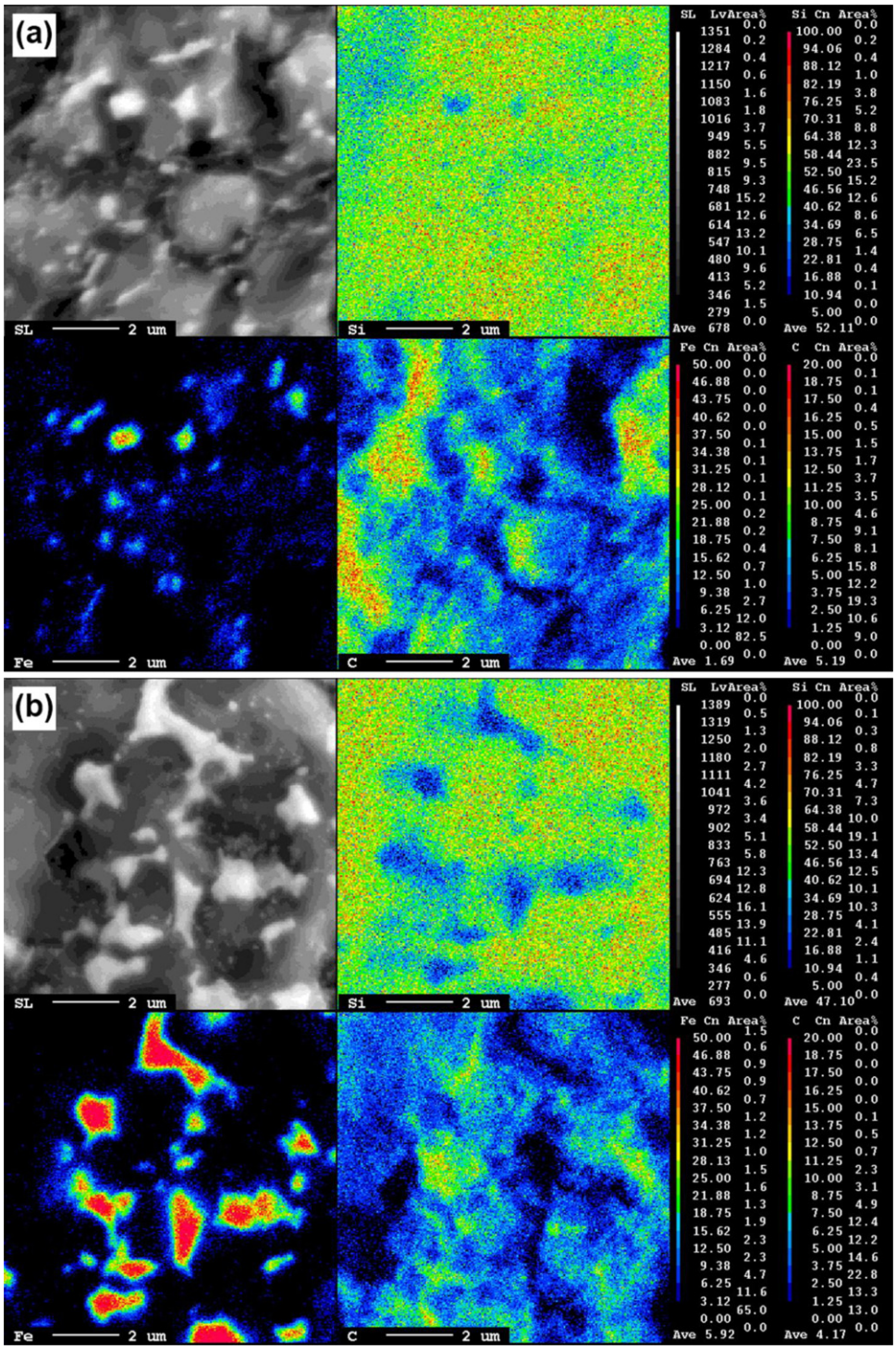

Fig. 4. Compositional maps of $Si_{1-x}Fe_xC$ samples: (a) $x = 0.01$ and (b) $x = 0.04$.

shell than their respective spin-splitting, leading to a preference for the low-spin state. Thus, for $Fe^{3+}(d^5)$ ion-substituted Si sites, four majority- and minority-spin *e*-states are filled first, and then a majority-spin t_2-state is filled by the fifth electron. Such an electronic configuration leads to a net magnetic moment per Fe ion of $1\,\mu_B$. If the $Fe^{3+}(d^5)$ ion is in the high-spin state, the expected magnetic moment is $5\,\mu_B$. Thus, the observed magnetic moment per Fe ion of $0.9\,\mu_B$ for the samples implies a preference for the low-spin state of the Fe *d* shell. For Fe_3Si, a magnetization measurement gives $0.86\,\mu_B$ per atom.[36]

Thus, the observed magnetization of the samples (Fig. 1) can be ascribed to two origins: ferromagnetic Fe_3Si crystallites and ferromagnetic alignment of individual magnetic moments of the Fe^{3+} ions randomly substituting the Si sites of the sample. Two interaction mechanisms are likely to be responsible for the latter: the Ruderman–Kittel–Kasuya–Yosida (RKKY) interaction

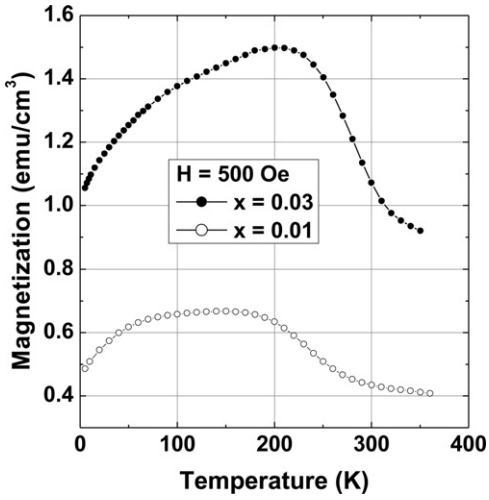

Fig. 5. Temperature dependence of the magnetization of $Si_{1-x}Fe_xC$ ($x = 0.01$ and 0.03) samples measured by SQUID under zero-field-cooled conditions and an external magnetic field of $H = 500$ Oe.

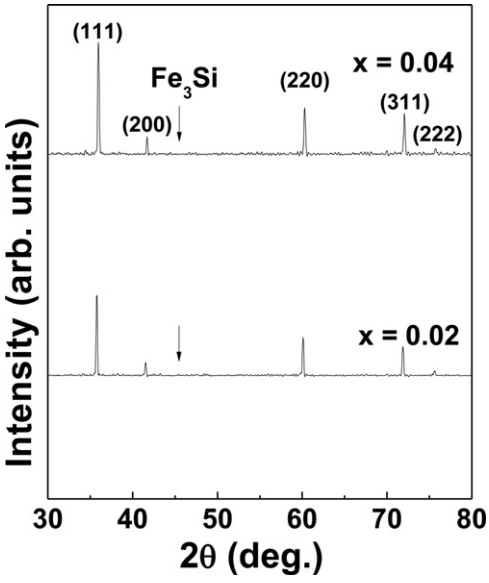

Fig. 6. XRD patterns of $Si_{1-x}Fe_xC$ ($x = 0.02$ and 0.04) samples after hydrochloric acid-leaching. Note the removal of Fe_3Si peaks.

and bound magnetic polaron (BMP) models.[23,24] The RKKY interaction needs free carriers in high density for the alignment of individual magnetic moments, while the BMP needs localized carriers. Song et al.,[25] based on their experimental results on Fe-doped 6H-SiC powders, concluded that the Fe_3Si phase in the samples is not the only origin for the observed ferromagnetism and suggested the RKKY mechanism as another possible reason. The estimated carrier density for effective RKKY interaction is $\sim 10^{21}$ cm^{-3} for SiC,[25] which is $\sim 10^2$ times larger than that of the present Fe-doped samples. Thus, the carrier-related magnetization of the samples is attributed to the formation of BMPs.

In Fig. 5, the temperature-dependent magnetization (zero-field-cooled) data, $M(T)$, for the $x = 0.01$ and 0.03 samples measured using SQUID under an external field of 500 Oe are compared. As expected from the existence of the ferromagnetic Fe_3Si phase in the samples, the $M(T)$ curves do not approach zero near 350 K where the Curie temperatures for SiC-based magnetic semiconductors are expected to be located. The values of $M(T)$ of $\sim$0.4 and $\sim$0.9 emu/cm^3 near 350 K for $x = 0.01$ and 0.03 samples ($\sim$60% of the maximum values), respectively, are attributed to the Fe_3Si crystallites. The observed decrease in magnetization with decreasing temperature in the low temperature region (below $\sim$100 K for $x = 0.01$ and $\sim$200 K for $x = 0.03$) implies a transition to the spin-glass phase.[37,38]

Therefore, the major contribution to the observed magnetization is ascribed to the ferromagnetic Fe_3Si crystallites in the Fe-doped SiC samples. The BMPs are likely to provide a minor contribution to the magnetization of the sample.

In order to decouple the contributions of the ferromagnetic Fe_3Si crystallites and the BMPs, Fe_3Si crystallite phase from Fe-doped SiC ($Si_{1-x}Fe_xC$) samples ($x = 0.02$ and 0.04) was removed by hydrochloric acid leaching.[31] Fig. 6 shows XRD patterns for the $x = 0.02$ and 0.04 samples after the leaching process. It is seen that the Fe_3Si-related peak at $2\theta = 45.3^\circ$ disappeared completely. Fig. 7 shows SEM images of the $x = 0.02$ and 0.04 samples after the leaching process. The comparison of Fig. 7 with Fig. 3(b) and (d) indicates that the ferromagnetic Fe_3Si phase acted as a bonding phase between SiC grains. By removing the bonding phase, the fracture mode changed from mostly transgranular to mostly intergranular fracture. In Fig. 8, the MH curves for $x = 0.02$ and 0.04 samples measured after the acid-leaching are compared

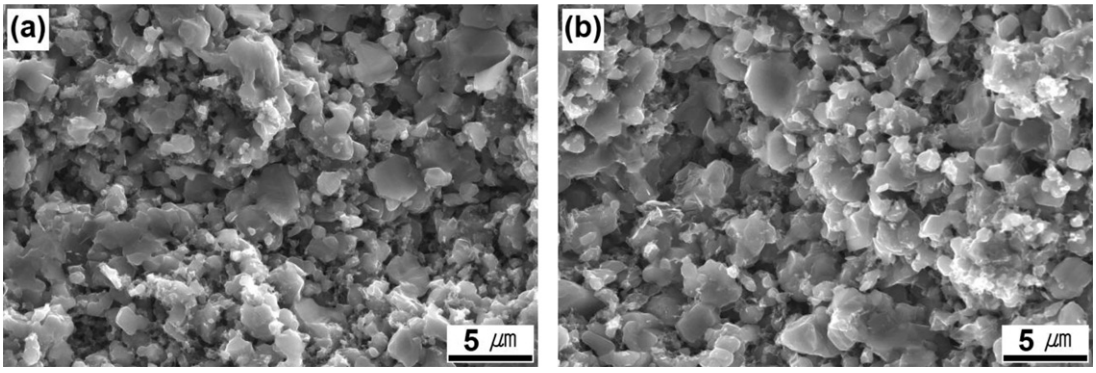

Fig. 7. SEM images of $Si_{1-x}Fe_xC$ samples after hydrochloric acid-leaching: (a) $x = 0.02$ and (b) $x = 0.04$.

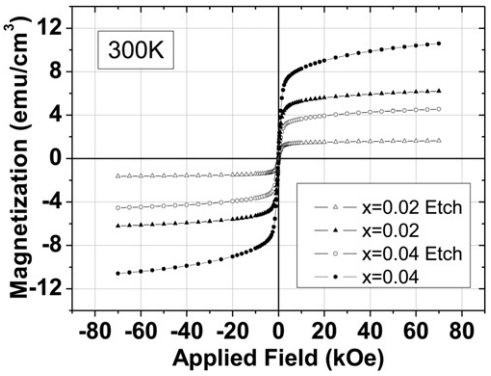

Fig. 8. Comparison of MH curves of $x = 0.02$ and 0.04 samples before and after acid-leaching measured using SQUID at 300 K.

with those before the leaching. The magnetization intensities at $H = 70$ kOe of the acid-leached samples were reduced compared to those before the leaching by 75% and 56% for the $x = 0.02$ and 0.04 samples, respectively. Thus, the comparison of SEM, XRD and MH results between the samples before and after the acid-leaching confirms the existence of segregated Fe_3Si phase in the Fe-doped SiC samples with its density increasing with the Fe content. Also, the residual magnetization in the samples after the leaching is interpreted as mainly due to the contribution of the BMPs to the ferromagnetism.

4. Conclusions

Bulk Fe-doped SiC ceramics with a zincblende structure exhibited ferromagnetic behavior at room temperature. The XRD and magnetic hysteresis results for the samples indicate the formation of a ferromagnetic Fe_3Si phase with its density increasing with x. The samples showed p-type conductivity with a hole concentration of $\sim 10^{19}$ cm^{-3} at room temperature, mainly attributable to Fe substitution into the Si sites. The observed magnetization of the Fe-doped SiC ceramics is mainly attributed to the Fe_3Si crystallites. Additionally, the minor contribution from the Fe^{3+} ions to the magnetization is likely through the formation of magnetic polarons bound with the holes.

Acknowledgments

The authors are sincerely grateful to Mr. Kwang-Young Lim (University of Seoul) for help with sample fabrication. This work was supported by the Mid-Career Researcher Program through a grant from the National Research Foundation of Korea (NRF) (No. 2010-0027502) funded by the Korean government (MEST).

References

1. Raynaud C. Silica films on silicon carbide: a review of electrical properties and device applications. *J Non-Cryst Solids* 2001;**280**:1–31.
2. Jenny JR, Malta DP, St. Muller G, Powell AR, Tsvetkov VF, McD Hobgood H, et al. High-purity semi-insulating 4H-SiC for microwave device applications. *J Electron Mater* 2003;**32**:432–6.
3. Siegelin F, Kleebe HJ, Sigl LS. Interface characteristics affecting electrical properties of Y-doped SiC. *J Mater Res* 2003;**18**:2608–17.
4. Nakamura D, Gunjishima I, Yamaguchi S, Ito T, Okamoto A, Kondo H, et al. Ultrahigh-quality silicon carbide single crystals. *Nature* 2004;**430**:1009–12.
5. Riccardi B, Giancarli L, Hasegawa A, Katoh Y, Kohyama A, Jones RH, et al. Issues and advances in SiC_f/SiC composites development for fusion reactors. *J Nucl Mater* 2004;**329–333**:56–65.
6. Estrada M, Cerdeira A, Resendiz L, Garcia R, Iniguez B, Marsal LF, et al. Amorphous silicon carbide TFTs. *Solid-State Electron* 2006;**50**:460–7.
7. Tabata S, Hirata Y, Sameshima S, Matsunaga N, Ijichi K. Liquid phase sintering and mechanical properties of SiC with rare-earth oxide. *J Ceram Soc Jpn* 2006;**114**:247–52.
8. Sajgalik P, Hnatko M, Lences Z, Dusza J, Kasiarova M. In situ preparation of Si_3N_4/SiC nanocomposites for cutting tool application. *Int J Appl Ceram Technol* 2006;**3**:41–6.
9. Janz S, Reber S, Lutz F, Schetter C. Conductive SiC as an intermediate layer for CSITF solar cells. *Thin Solid Films* 2006;**511–512**:271–4.
10. Balog M, Sajgalik P, Hofer F, Warbichler P, Frohlich K, Vavra O, et al. Electrically conductive SiC–$(Nb,Ti)_{ss}$–$(Nb,Ti)C_{ss}$ cermet. *J Eur Ceram Soc* 2006;**26**:1259–66.
11. Can A, Herrmann M, Mclachlan DS, Sigalas I, Adler J. Densification of liquid phase sintered silicon carbide. *J Eur Ceram Soc* 2006;**26**:1707–13.
12. Melinon P, Masenelli B, Tournus F, Perez A. Playing with carbon and silicon at the nanoscale. *Nat Mater* 2007;**6**:479–90.
13. Can A, Mclachlan DS, Sauti G, Herrmann M. Relationships between microstructure and electrical properties of liquid-phase sintered silicon carbide materials using impedance spectroscopy. *J Eur Ceram Soc* 2007;**27**:1361–3.
14. Kim YW, Chun YS, Nishimura T, Mitomo M, Lee YH. High-temperature strength of silicon carbide ceramics sintered with rare-earth oxide and aluminum nitride. *Acta Mater* 2007;**55**:727–36.
15. Wang J, Zhao T, Li J, Huang AQ, Callanan R, Husna F, et al. Characterization, modeling, and application of 10-kV SiC MOSFET. *IEEE Trans Electron Devices* 2008;**55**:1798–806.
16. Hirata Y, Matsunaga N, Hidaka N, Tabata S, Sameshima S. Processing of high performance silicon carbide. *J Ceram Soc Jpn* 2008;**116**:665–73.
17. Ning L, Feng Z, Wang Y, Zhang K, Feng Z. Vanadium-doped semi-insulating 6H-SiC for microwave power device applications. *J Mater Sci Technol* 2009;**25**:102–4.
18. Liu F, Carraro C, Pisano AP, Maboudian R. Growth and characterization of nitrogen-doped polycrystalline 3C-SiC thin films for harsh environment MEMS applications. *J Micromech Microeng* 2010;**20**:035011.
19. Hirata Y, Suzue N, Matsunaga N, Sameshima S. Particle size effect of starting SiC on processing, microstructure and mechanical properties of liquid phase-sintered SiC. *J Eur Ceram Soc* 2010;**30**:1945–54.
20. Rodriguez-Rojas F, Ortiz AL, Guiberteau F, Nygren M. Anomalous oxidation behavior of pressureless liquid-phase-sintered SiC. *J Eur Ceram Soc* 2011;**31**:2393–400.
21. Xi G, Yu S, Zhang R, Zhang M, Ma D, Qian Y. Crystalline silicon carbide nanoparticles encapsulated in branched wavelike carbon nanotubes: synthesis and optical properties. *J Phys Chem B* 2005;**109**:13200–4.
22. Kim YW, Kim KJ, Kim HC, Cho NH, Lim KY. Electrodischarge-machinable silicon carbide ceramics sintered with yttrium nitrate. *J Am Ceram Soc* 2011;**94**:991–3.
23. Dietl T, Ohno H, Matsukura F, Cibert J, Ferrand D. Zener model description of ferromagnetism in zinc-blende magnetic semiconductors. *Science* 2000;**287**:1019–22.
24. Coey JMD, Venkatesan M, Fitzgerald CB. Donor impurity band exchange in dilute ferromagnetic oxide. *Nat Mater* 2005;**4**:173–8.
25. Song B, Jian JK, Li H, Lei M, Bao HQ, Chen XL, et al. New experimental evidence for origin of ferromagnetism ordering in Fe-doped SiC. *Physica B* 2008;**403**:2897–901.
26. Wang W, Takano F, Ofuchi H, Akinaga H. Magnetic properties of transparent SiC:Mn films synthesized on SiC substrates. *J Magn Magn Mater* 2007;**310**:2141–3.
27. Takano F, Wang W, Akinaga H, Ofuchi H, Hishiki S, Ohshima T. Characterization of Mn-doped 3C-SiC prepared by ion implantation. *J Appl Phys* 2007;**101**:09N510.

28. Song GS, Kobayashi M, Hwang JI, Kataoka T, Takizawa M, Fujimori A, et al. X-ray absorption and photoemission studies of ferromagnetic Mn-implanted 3C-SiC. *Jpn J Appl Phys* 2008;**47**:7113–6.
29. Los AV, Timoshevskii AN, Los VF, Kalkuta SA. Ab initio studies of magnetism in transition-metal-doped silicon carbide. *Phys Rev B* 2007;**76**:165204.
30. Liu Y, Wang G, Wang S, Yang J, Chen L, Qin X, et al. Defect-induced magnetism in neutron irradiated 6H-SiC single crystal. *Phys Rev Lett* 2011;**106**:087205.
31. Santos IC, Goncalves AP, Santos CS, Almeida M, Afonso MH, Cruz MJ. Purification of metallurgical grade silicon by acid leaching. *Hydrometallurgy* 1990;**23**:237–46.
32. Chikazumi S. *Physics of ferromagnetism*. New York: Oxford University Press; 1997. p. 227.
33. Kuryliszyn-Kudelska I, Diduszko R, Tymicki E, Dobrowolski W, Grasza K. Magnetic properties of Fe doped SiC crystals. *Phys Stat Sol (b)* 2007;**244**:1743–6.
34. Rein RH, Chipman J. The free energy of SiC from its solubility in Fe and from gas–solid equilibria with SiO_2, graphite, and CO. *J Phys Chem* 1963;**67**:839–41.
35. Miao MS, Lambrecht WRL. Electronic structure and magnetic properties of transition-metal-doped 3C and 4H silicon carbide. *Phys Rev B* 2006;**74**:235218.
36. Vinzelberg H, Schumann J, Elefant D, Arushanov E, Schmidt OG. Transport and magnetic properties of Fe_3Si epitaxial films. *J Appl Phys* 2008;**104**:093707.
37. Shand PM, Christianson AD, Pekarek TM, Martinson LS, Schweitzer JW, Miotkowski I, et al. Spin-glass ordering in the diluted magnetic semiconductor $Zn_{1-x}Mn_xTe$. *Phys Rev B* 1998;**58**:12876–82.
38. Torres T, Sagredo V, Chalbaud LM, Attolini G, Bolzoni F. Magnetic and structural characterization of the semiconductor $FeIn_2Se_4$. *Physica B* 2006;**384**:100–2.